Spin conversion of positronium in NiO/Al_2O_3 catalysts observed by coincidence Doppler broadening technique

H. J. Zhang, Z. Q. Chen,*,† and S. J. Wang*,‡
Hubei Nuclear Solid Physics Key Laboratory, Department of Physics, Wuhan University, Wuhan 430072, People's Republic of China

A. Kawasuso and N. Morishita
Advanced Science Research Center, Japan Atomic Energy Agency, 1233 Watanuki, Takasaki, Gunma 370-1292, Japan
(Received 30 April 2010; revised manuscript received 6 July 2010; published 28 July 2010)

High-purity NiO/Al_2O_3 catalysts were prepared by mixing NiO and γ-Al_2O_3 nanopowders. X-ray diffraction patterns were measured to characterize the grain size and crystalline phase of the nanopowders. Positron-annihilation spectroscopy was used to study the microstructure and surface properties of the pores inside the NiO/Al_2O_3 catalysts. The positron lifetime spectrum comprises two short and two long lifetime components. The two long lifetimes τ_3 and τ_4 correspond to ortho-positronium (o-Ps) annihilated in microvoids and large pores, respectively. With increasing NiO content in the NiO/Al_2O_3 catalysts, both τ_4 and its intensity I_4 show continuous decrease. Meanwhile, the para-positronium (p-Ps) intensity, obtained from coincidence Doppler broadening spectra, increases gradually with NiO content. The different variation in o-Ps and p-Ps intensity suggests the ortho-para conversion of positronium in NiO/Al_2O_3 catalysts. X-ray photoelectron spectroscopy shows that Ni mainly exists in the form of NiO. The electron-spin-resonance measurements reveal that the ortho-para conversion of Ps is induced by the unpaired electrons of the paramagnetic centers of NiO.

DOI: 10.1103/PhysRevB.82.035439 PACS number(s): 78.70.Bj, 82.30.Gg, 36.10.Dr

I. INTRODUCTION

NiO/Al_2O_3 catalysts are very important in technological processes, such as methane-steam reforming, methanol reforming, hydrodesulphurization, hydrodenitrogenation, and hydrocarbon cracking.[1,2] The catalytic property is influenced by various factors, such as the specific surface area, pore structure, and dispersion of the active component on the support.[3] The pore structure of the catalyst support is most important because it provides passage for both reactants and resultants and affects the speed and efficiency of reaction. However, up to now very limited research works were focused on the pore structure of catalysts. Few techniques are capable of probing the nanometer-sized pores. This is particularly true if the pores are not interconnected so that the gas absorption techniques fail to work.

Positron is a self-seeking probe for vacancy-type defect in solids. In porous materials, the positronium (Ps) atom, the bound state of positron and electron, will be formed in the pores where the electron density is sufficiently low. According to the spins of the electron and positron, the Ps atom exists in two states: the singlet spin state para-Ps (p-Ps) ($S=0$, $m_S=0$) and the triplet spin state ortho-Ps (o-Ps) ($S=1$, $m_S=0, \pm 1$). The ratio of p-Ps to o-Ps formation probability is 1:3 in vacuum. The p-Ps mostly undergoes self-annihilation (annihilates with its own electron) by emitting two γ rays while o-Ps annihilates into three γ rays in vacuum. The self-annihilation lifetime of p-Ps and o-Ps is 125 ps and 142 ns, respectively. When Ps is formed in porous media, the o-Ps inside pores will annihilate with the surface electrons of the pores into two γ rays, which is called pick-off annihilation process, and the annihilation lifetime of o-Ps will be largely reduced. Good correlation between o-Ps lifetime and the radius of the pore have been established three decades ago.[4] In addition, the o-Ps will react with some chemical agents on the wall of the pore, which could also reduce the o-Ps lifetime and its formation probability. Therefore positron-annihilation lifetime measurement is a powerful way to characterize the pore structure and surface properties of porous materials.

Except for the positron lifetime measurements which could reveal the pore structure information, the Doppler broadening of positron-annihilation radiation reflects the momentum distributions of electrons with which positron annihilates. When the Ps is formed in porous media, the self-annihilation radiation of p-Ps will contribute a narrow peak to the Doppler broadening spectrum because of its almost zero momentum. Therefore Doppler broadening measurements can be also used to monitor the p-Ps component. The recently developed coincidence Doppler broadening (CDB) technique could greatly reduce the noisy background by using two Ge detectors, thus increases the accuracy of electron momentum distribution.[5]

Gamma-alumina (γ-Al_2O_3) is known to be a kind of catalyst support due to the excellent textural properties (surface area, pore volume, pore-size distribution, and acid/base characteristics), the chemical and hydrothermal stability.[3] The nanometer-sized γ-Al_2O_3 has even higher specific surface area and therefore is expected to have better performance. In this paper, we prepared the NiO/Al_2O_3 catalysts by solid-state reaction method using pure γ-Al_2O_3 and NiO nanopowders. The pore structure and surface properties of the catalysts were studied using positron annihilation, x-ray photoelectron spectroscopy (XPS), and electron-spin-resonance (ESR) measurements.

II. EXPERIMENT

Samples for this study were prepared from commercially available high-purity NiO (grain size ~30 nm, purity

>99.9%) and γ-Al_2O_3 (grain size ~20 nm, purity >99.96%) nanopowders. The two powders were mixed together with NiO content varying from 3 to 40 wt %. The mixed powder were hand milled in agate mortar with pestle for 2 h and then pressed into pellets under a static pressure of about 6 MPa for 5 min at room temperature. The pellet samples were in disk shape having a diameter of 15 mm and thickness of ~2 mm. Before any measurements, the pellets were dried in the electric furnace at 100 °C for 2 h.

The positron lifetime and coincidence Doppler broadening spectra were measured simultaneously at room temperature by putting the two lifetime detectors perpendicular to the two high-purity Ge detectors. A ^{22}Na positron source (~5 μCi) was sandwiched between two identical sample pellets and was put in a sample chamber. The sample chamber was evacuated by a turbo molecular pump and the vacuum inside the sample chamber is better than 1×10^{-5} torr.

The positron lifetime was measured using a conventional fast-fast coincidence system. The time resolution of the lifetime system is about 280 ps. The time range of the time-to-amplitude converter was set to 500 ns for pure γ-Al_2O_3 sample and 200 ns for other samples. The total channel number is 4096, and the time scale is 50.7 and 126.8 ps/channel for the two time ranges, respectively. There is no difference in the positron lifetime result for pure γ-Al_2O_3 measured using 200 and 500 ns time range. Each spectrum was collected with a total count of 1×10^6 and at least two spectra were measured for each sample.

The coincidence Doppler broadening system consists of two high-purity germanium detectors with energy resolution of about 1.76 and 1.64 keV full width at half maximum (FWHM) at 1.33 MeV, which corresponds to an energy resolution of about 1.3 and 1.1 keV at 511 keV, respectively. The source sample sandwich was placed in the middle of the two detectors. The two annihilation γ rays with energy E_1 and E_2 were recorded by each one detector, respectively. Two-dimensional Doppler broadening spectra were recorded using a FastComTec multiparameter system with a total count of about 1×10^7 and the count rate was about 50/s. The difference of E_1 and E_2, $\Delta E = E_1 - E_2$, equals to cP_L, where c is the speed of light, P_L is the longitudinal component of the positron-electron momentum along the direction of the γ-ray emission. The one-dimensional coincidence Doppler broadening spectra was obtained by projecting the two-dimensional data onto the $E_1 - E_2$ axis. A window of $2m_0c^2 - 2.0$ keV $< E_1 + E_2 < 2m_0c^2 + 2.0$ keV (m_0 is the rest mass of free electron) along the diagonal was chosen to remove any irrelevant noisy signals. The final spectrum has a total channel number of 1023 with energy scale of 35.7 eV/channel and the peak to background ratio is about 1×10^5.

The one-dimensional Doppler broadening spectrum was characterized using the S and W parameters. The S parameter is defined as the ratio of low-momentum ($|P_L| < 0.68$ keV) region to the total region of the spectrum and the W parameter is defined as the ratio of high momentum ($2.86 < |P_L| < 5.73$ keV) region to the total region.

X-ray diffraction (XRD) measurements were performed using Cu $K\alpha$ radiation (Bruker D8 Advance) with a Ni filter. The scanning rate was 1 °/min with a step of 0.02°. XPS measurements were performed using a model XSAM800 ESCA spectrometer (KRATOS Product, Britain). XPS employed Mg $K\alpha$ (1253.6 eV) excitation source, with a voltage of 12.5 kV and an emission current of 16 mA at a base pressure of 2×10^{-7} Pa. The spectrometer was run in fix retard ratio (FRR) mode. Excitation and emission spectra were measured by a Shimadzu RF-5301PC spectrometer. The binding energies were calibrated against the C_{1s} peak at 284.8 eV. ESR spectra were measured with an RE-3X (JEOL) at room temperature using the microwave X-band frequency (9.4390 GHz). In all ESR measurements, the magnetic field was swept in the range of 436.9 ± 400 mT with a field modulation of 0.2 mT, time constant of 0.1 s, sweep time of 8 min, and microwave power of 0.1 mW. ESR signal parameters were analyzed using the ES-IPRIT (JEOL Datum, Hachioji) software program.

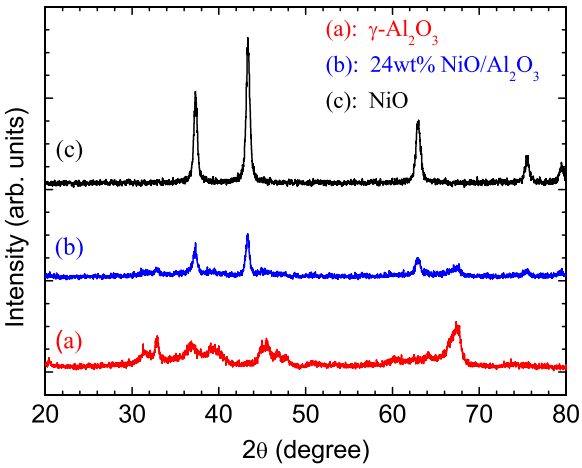

FIG. 1. (Color online) XRD patterns for (a) γ-Al_2O_3, (b) 24 wt % NiO/Al_2O_3, and (c) NiO.

III. RESULTS AND DISCUSSION

A. XRD measurement

To study the grain size and the crystalline phase of the nanopowders, three samples were subjected to x-ray diffraction analyses. The samples selected were: γ-Al_2O_3, NiO and 24 wt % NiO/Al_2O_3. The XRD patterns are shown in Fig. 1. The diffraction lines of pure γ-Al_2O_3 (JCPDS Card No. 47–1308) and NiO nanocrystals (JCPDS Card No. 04–0835) can be identified. The NiO sample shows better crystallinity than γ-Al_2O_3. For the 24 wt % NiO/Al_2O_3 catalysts, the observed peaks can be indexed with the γ-Al_2O_3 and cubic NiO phase. The other phase such as Ni_2O_3 or $NiAl_2O_4$ spinel is not observed.

The average grain size of the samples is calculated by Scherrer's formula[6]

$$D_{hkl} = K\lambda/\beta \cos\theta, \quad (1)$$

where D_{hkl} is the average grain size perpendicular to (hkl) plane, K is the shape factor (usually taken as 0.89), λ is taken as the x-ray wavelength of Cu $K_{\alpha 1}$ radiation ($\lambda = 0.15418$ nm), β is the FWHM of the XRD peak (every

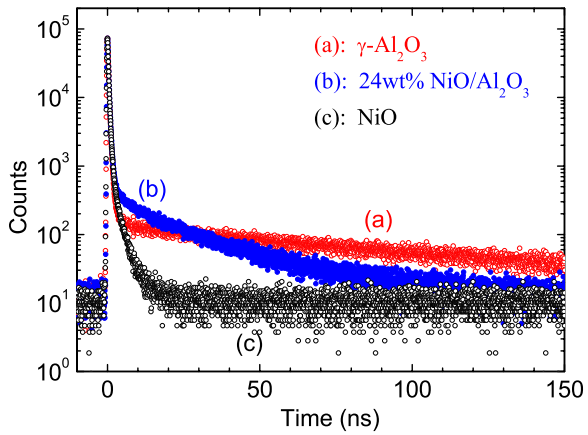

FIG. 2. (Color online) Peak-normalized positron lifetime spectrum of (a) γ-Al_2O_3, (b) 24 wt % NiO/Al_2O_3, and (c) NiO.

observed peak in the spectra was fitted with a Gaussian function), and θ is the Bragg angle. Standard method to deduct the contribution of instrumental broadening in FWHM has been taken into account. The average grain sizes derived by Scherrer's formula were about 19 nm for γ-Al_2O_3, 21 nm for 24 wt % NiO/Al_2O_3, and 23 nm for NiO, respectively.

B. Positron lifetime measurements

Positron lifetime spectra were measured for all the samples, including pure γ-Al_2O_3, pure NiO, and NiO/Al_2O_3 samples with different NiO content. Figure 2 shows the peak-normalized positron lifetime spectra of γ-Al_2O_3, NiO, and 24 wt % NiO/Al_2O_3. It is obvious that there is a rather long lifetime in the spectrum of pure γ-Al_2O_3. While in pure NiO, the lifetime is much shorter. The positron lifetime in 24 wt % NiO/Al_2O_3 is between that of the two pure samples. All the positron lifetime spectra were analyzed using the PATFIT program.[7] Due to the long positron lifetime in all the samples, the background of the spectrum was subtracted using the average count before the lifetime peak. The lifetimes and relative intensities of the above three samples are listed in Table I.

In pure γ-Al_2O_3, four lifetime components could be resolved from the lifetime spectrum. The shortest lifetime component τ_1 (153 ps) is attributed to p-Ps annihilation[8] and free positron annihilation. The intermediate component τ_2 (410 ps) is due to annihilation of positrons trapped in the vacancy clusters and voids. The longer lifetime τ_3 (2.4 ns) corresponds to o-Ps annihilation in some microvoids which might exist inside Al_2O_3 grains. The ultralong lifetime τ_4 (93.7 ns) is attributed to o-Ps annihilation in the large pores which are distributed between nanograins.[9] The intensities of the two long o-Ps lifetime components are 1.4% and 21.4%, respectively. Shek *et al.*[10] have also measured positron lifetime in amorphous and polycrystalline nanometer-sized alumina. They obtained three lifetime components: the shortest lifetime τ_1 (170 ps), the intermediate lifetime τ_2 (410 ps), and the long lifetime τ_3 (1.7–5.0 ns). However, they did not observe the longer o-Ps lifetime. The reason might be due to their different sample preparation method, experiment setup for the lifetime spectrometer, such as the time range, energy window of the annihilation γ ray, and the analysis of the lifetime spectra.

The mean void radius R can be estimated from the measured o-Ps lifetime by using a semiempirical equation based on a spherical infinite potential-well model (Tao-Eldrup model),[4,11] resulting in the following equation:

$$\tau_{\text{o-Ps}}^{-1} = 2\left[1 - \frac{R}{R+\Delta R} + \frac{1}{2\pi}\sin\left(2\pi\frac{R}{R+\Delta R}\right)\right], \qquad (2)$$

where ΔR is the thickness of the electron layer on the surface of pores, which is an empirical parameter (0.1656 nm) determined by fitting the well-known free volume.[12] This equation is valid only for o-Ps lifetimes shorter than 20 ns.[13] For longer o-Ps lifetime such as the almost 100 ns component in the γ-Al_2O_3, the self-annihilation of o-Ps cannot be neglected. Due to the large pore size, the overlap of the positron wave function with the electron layer on the pore surface is reduced and most of the o-Ps will undergo self-annihilation by emitting 3 γ rays with a rather long lifetime. Ito *et al.*[14] extended the above Tao-Eldrup model to estimate larger void radius from the o-Ps lifetime data by considering the o-Ps intrinsic three γ annihilations in the center of the void, in addition to the o-Ps pick-off annihilations within an electron layer on the void wall

$$\tau_{\text{o-Ps}}^{-1} = 2\left[1 - \frac{R_a}{R_a+\Delta R} + \frac{1}{2\pi}\sin\left(\frac{2\pi R_a}{R_a+\Delta R}\right)\right] \times\left[1 - \left(\frac{R-R_a}{R+\Delta R}\right)^b\right] + \frac{1}{142}, \qquad (3)$$

where R_a (0.8 nm) and b (0.55) are fitted parameters, and ΔR is the empirical parameter (0.1656 nm) shown in Eq. (2). By combining Eqs. (2) and (3), we can obtain the mean diameter of microvoids and large pores in γ-Al_2O_3 nanopowders, which are 0.64 nm and 18.4 nm, respectively.

In pure NiO nanopowders, there are also four positron lifetime components, with two short lifetime τ_1=243 ps, τ_2 =573 ps, and two long lifetime τ_3=3.67 ns, τ_4=43.8 ns. But the intensity of the two long lifetime component is rather small, which is around 4.0% and 3.8%, respectively. In the 24 wt % NiO/Al_2O_3 sample, it is also easy to find that the

TABLE I. Positron lifetimes and relative intensities in pure γ-Al_2O_3, NiO, and 24 wt % NiO/Al_2O_3.

Sample	τ_1/ps (I_1/%)	τ_2/ps (I_2/%)	τ_3/ns (I_3/%)	τ_4/ns (I_4/%)
γ-Al_2O_3	152.8±3.4 (36.8±1.0)	410.2±5.2 (40.4±0.9)	2.35±0.15 (1.4±0.1)	93.7±0.6 (21.4±0.1)
24 wt % NiO/Al_2O_3	167.8±3.1 (42.1±0.9)	445.7±4.9 (39.8±0.9)	6.35±0.21 (4.1±0.1)	31.7±0.3 (14.1±0.1)
NiO	242.8±2.5 (72.2±1.2)	573.1±15.5 (20.0±1.1)	3.67±0.08 (4.0±0.1)	43.8±0.7 (3.8±0.1)

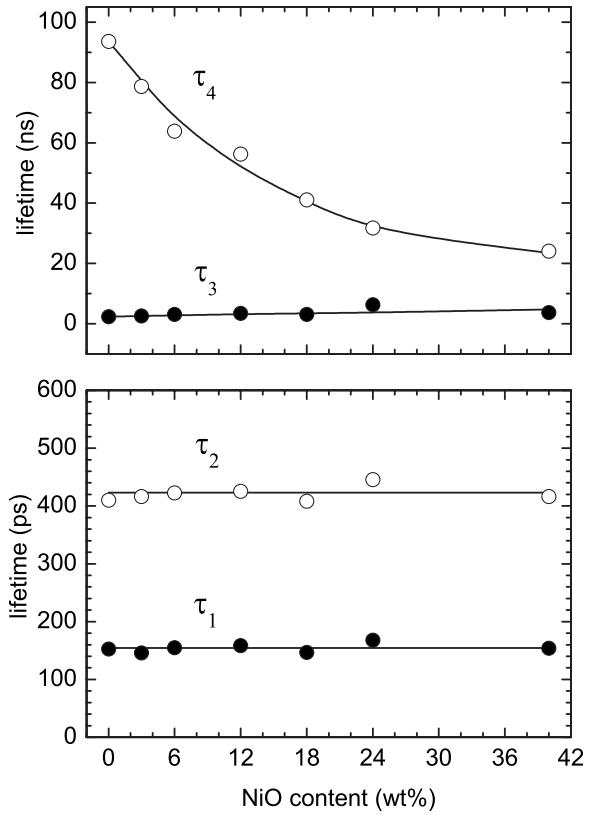

FIG. 3. Variation in the four lifetime components as a function of the NiO content.

long lifetime component decreases sharply to 31.7 ns and its intensity drops to 14.1%. Figure 3 shows the variation in the four lifetime components of NiO/Al_2O_3 catalysts as a function of the NiO content in weight percentage. With increasing NiO content from 0 to 40 wt %, τ_1 and τ_2 keep almost unchanged while τ_3 shows slight increase from 2.35 to 3.74 ns. However, for the longest lifetime τ_4, it decreases significantly from 93.7 to 24.1 ns when the NiO content increases to 40 wt %. Figure 4 shows the variation in the intensities I_4,

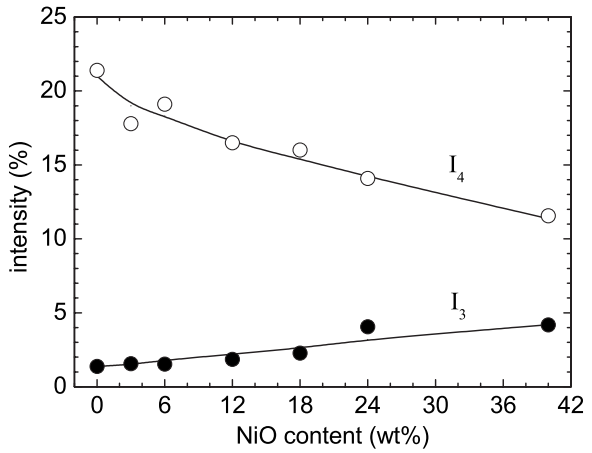

FIG. 4. Variation in I_4 and I_3 as a function of the NiO content.

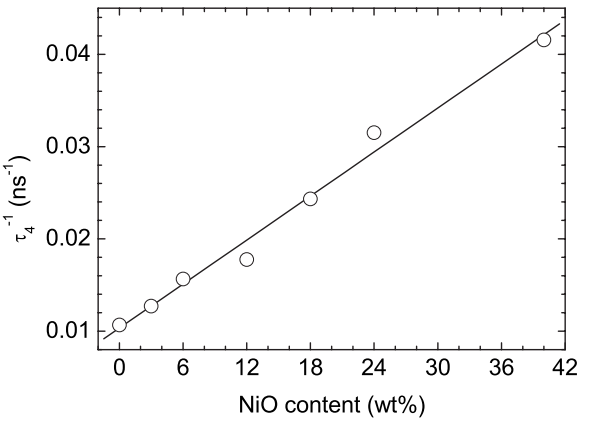

FIG. 5. Reciprocal of the o-Ps lifetime τ_4 as a function of the NiO content.

I_3 as a function of NiO content. I_4 shows also significant decrease from 21.4% to 11.6% while I_3 increases slightly from 1.4% to 4.2%.

The decrease in τ_4 might be caused by the decrease in the pore size. However, the large pores are unoccupied space between nanosized grains. The average grain sizes of γ-Al_2O_3 and NiO were derived to be 19 and 23 nm by Scherrer's formula from the XRD measurement, which are close to each other. All the mixed nanopowders were pressed at the same condition, so the size of large pores in NiO/Al_2O_3 should have no significant change with increasing NiO content. Thus the decrease in τ_4 is probably due to other reasons, such as the quenching effect by some active centers on the surface of the pore. In pure γ-Al_2O_3, the pores were surrounded only by γ-Al_2O_3 grains. With the addition of NiO, the pores were surrounded by both γ-Al_2O_3 and NiO grains. Some NiO grains on the surface of the pore will interact with o-Ps and reduce its lifetime and intensity. It is also noteworthy that τ_3 does not show significant change with NiO content. This is because that the NiO grain size is much larger than the microvoid in γ-Al_2O_3 (0.64 nm in diameter). On the contrary, due to the decrease in τ_4, the difference between τ_4 and τ_3 becomes small, therefore the resolved τ_3 and I_3 both show slight increase.

The change in the o-Ps annihilation rate $\lambda_{o\text{-}Ps}$ (reciprocal of o-Ps lifetime) as a result of quenching effect can be expressed by the following equation:

$$\lambda_{o\text{-}Ps} = \lambda^0_{o\text{-}Ps} + k[M], \tag{4}$$

where $\lambda^0_{o\text{-}Ps}$ is the o-Ps annihilation rate without quenching effect, $[M]$ is the mass content percentage of the reactant reacting with Ps, and k is a constant. We plotted in Fig. 5 the variation in λ_4 $(=1/\tau_4)$ as a function of the NiO content. It is very clear that the data can be well fitted by a straight line. The slope of the fitting line, i.e., the constant k, is $(7.9 \pm 0.4) \times 10^7$ s^{-1}.

The quenching of o-Ps may have several possible origins, such as spin conversion through electron exchange and chemical quenching effect.[15] For spin-conversion process, the o-Ps exchanges one electron (which has spin opposite to that of the positron) with surrounding paramagnetic mol-

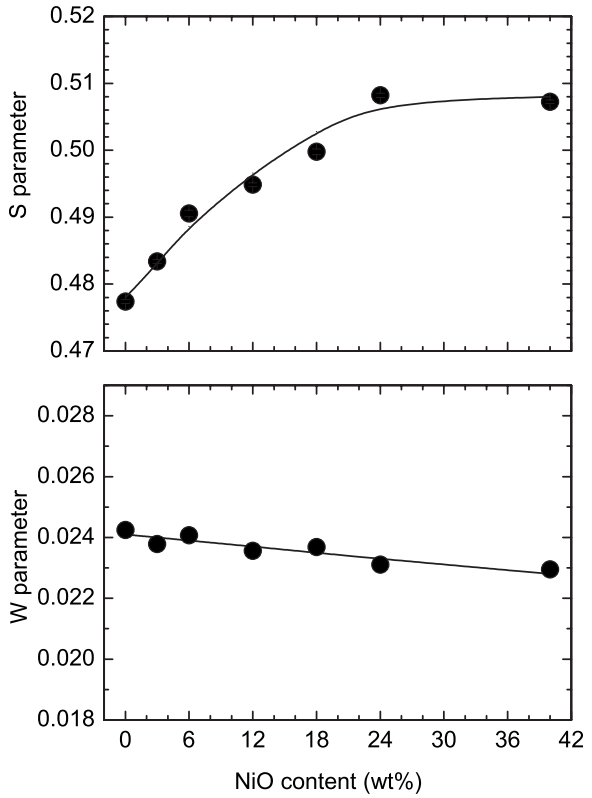

FIG. 6. Variation in *S* and *W* parameters as a function of the NiO content.

ecule, thus the o-Ps is converted to p-Ps and then undergoes self-annihilation by 2γ emission. In the chemical quenching process, the o-Ps will combine with some molecules and annihilate from this bound state. Both processes will result in a decrease in both o-Ps lifetime and its intensity. Therefore from only the positron lifetime measurements we cannot clarify which process is responsible for the change in τ_4 and I_4.

C. Coincidence Doppler broadening measurements

In order to further clarify the quenching process of o-Ps in the NiO/Al_2O_3 catalysts, we also performed coincidence Doppler broadening measurements at the same time. This measurement is necessary to separate spin conversion and other chemical reaction of positronium. The *S* and *W* parameters derived from the coincidence Doppler spectrum as a function of the NiO content are shown in Fig. 6. *S* parameters increase continuously from 0.48 to 0.51 with increasing NiO content up to 24 wt %, and then keep unchanged, while *W* parameters show only slight decrease from 0.024 to 0.023.

The increase in *S* parameter is not in consistence with the decrease in τ_4 and I_4. Generally, decrease in the o-Ps lifetime and intensity will induce decrease in *S* parameter. Since the formation of o-Ps to p-Ps probability is 3:1, decrease in o-Ps intensity implies that p-Ps intensity also decreases. As p-Ps contains nearly zero momentum, its self-annihilation will add a narrow peak to the Doppler broadening spectrum. For this reason, the change in *S* parameter is generally similar to the change in o-Ps intensity.

The increase in *S* parameter in our results thus might be due to an increase in the p-Ps intensity. Despite that the angular correlation of positron-annihilation radiation (ACAR) is the most appropriate method to study the p-Ps formation because of its better angular resolution, Doppler broadening measurements has the advantage of much faster data collection, relatively weak source strength requirements, and much simpler experimental setup. Especially the coincidence Doppler broadening technique improves its energy resolution by a factor of $\sqrt{2}$ and increases the peak to background ratio to more than 10^5, which makes it a good substitution for ACAR measurements. The effect of energy resolution on Doppler broadening spectrum can further be partly removed by a deconvolution process. Figure 7 shows the deconvoluted coincidence Doppler broadening spectra for pure γ-Al_2O_3, 6 wt % NiO/Al_2O_3, 12 wt % NiO/Al_2O_3, and 24 wt % NiO/Al_2O_3. The energy resolution of the coincidence Doppler broadening system is assumed to be around 0.9 keV from the single detector resolution of 1.3 and 1.1 keV. A point by point deconvolution method was used.[16] In pure γ-Al_2O_3, the p-Ps narrow peak can be just seen but not so clear. However, with the addition of only 6 wt % NiO, the p-Ps peak becomes apparent. With increasing NiO content, the intensity of p-Ps signal shows continuous increase, and the width of this peak also becomes narrower.

To further confirm the increase in p-Ps intensity, we need to analyze the coincidence Doppler broadening spectra in more details. It is possible to obtain the p-Ps intensity by utilizing a multi-Gaussian fitting[17–19] of Doppler broadening spectrum using the ACARFIT program included in the PATFIT package.[7] In order to check the reliability of multi-Gaussian fitting to obtain p-Ps intensity, we measured a series of polymer samples using both CDB and conventional positron lifetime measurements. The polymers selected were: polyamide 6, polypropylene, polyethylene, Linear low-density polyethylene, polycarbonate, and polystyrene. The p-Ps intensity obtained from CDB measurements showed very good agreement with that of positron lifetime measurements (1/3 of o-Ps intensity), which is similar to the result reported before.[20]

In pure γ-Al_2O_3 nanopowders, three Gaussian components can be resolved from the Doppler spectrum. The narrowest component has a width (FWHM) of 1.16 keV, which is obviously the p-Ps component. The rather narrow momentum distribution of p-Ps reflects that the pores seen by p-Ps has large open volume.[21,22] The intensity of the p-Ps component is about 10.2%. While the total o-Ps intensity (I_3+I_4) obtained from positron lifetime measurements is around 22.8%, the ratio of o-Ps to p-Ps intensity in γ-Al_2O_3 is 2.24, which is a little smaller than 3. This might be due to the incomplete measurement of the o-Ps 3γ annihilation events by positron lifetime system. The narrow energy window of the constant fraction differential discriminator in the lifetime measurement system will inevitably exclude some 3γ events. In Fig. 8 we plotted the variation in p-Ps and total o-Ps intensity as a function of NiO content in NiO/Al_2O_3 catalysts. In contrast to the decrease in the o-Ps intensity, the p-Ps intensity shows increase from 10.2% to almost 16%. The ratio of o-Ps to p-Ps intensity decreases to nearly 1. This

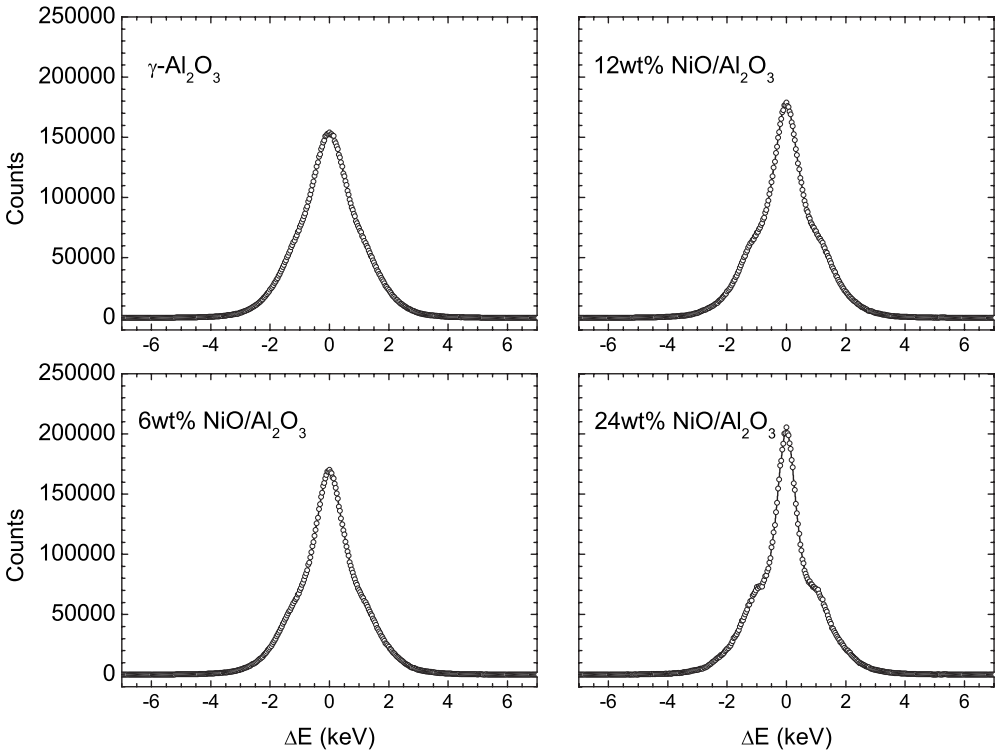

FIG. 7. Deconvoluted coincidence Doppler broadening spectra for pure γ-Al_2O_3, 6 wt % NiO/Al_2O_3, 12 wt % NiO/Al_2O_3, and 24 wt % NiO/Al_2O_3. All the spectra are normalized to a total count of 10^7.

clearly indicates that the quenching of o-Ps is due to spin conversion of Ps (the conversion from o-Ps to p-Ps).[23] With increasing NiO content up to 40 wt %, the width of p-Ps component of Doppler spectrum also decreases to less than 1.0 keV, which is in agreement with the result in Fig. 7. The narrowing of p-Ps component is probably induced by the contribution of converted o-Ps, which has survived tens of nanoseconds and therefore had more time than p-Ps to lose energy by collisions with the walls of the pore.

D. XPS and ESR results

XPS was used to provide information about the oxidation state and the chemical environment of the Ni species in NiO/Al_2O_3 catalyst. The samples selected for XPS analyses were: 6 wt %, 12 wt %, and 24 wt % NiO/Al_2O_3. The background-subtracted Ni $2p_{3/2}$ XPS spectra of the three samples are shown in Fig. 9. The curve fitting was carried out with a mixed Lorentzian-Gaussian function.

The electron binding energy of Ni $2p_{3/2}$ determined by XPS was about 854.8 eV for all the three samples. With increasing NiO content, a shake-up satellite peak of Ni $2p_{3/2}$ can be seen at about 6.5 eV higher binding energy. According to the previous literatures, the electron-binding energy of

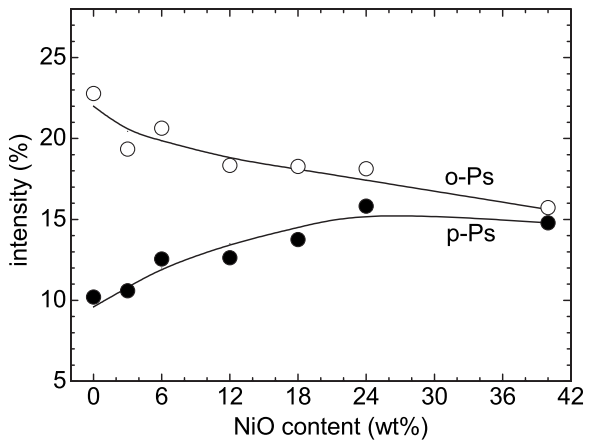

FIG. 8. Variation in o-Ps and p-Ps intensity in NiO/Al_2O_3 as a function of the NiO content.

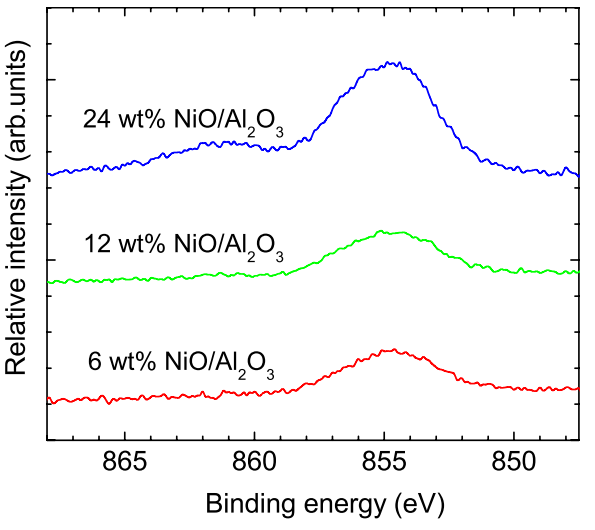

FIG. 9. (Color online) XPS spectra of Ni $2p_{3/2}$ region for 6 wt % NiO/Al_2O_3, 12 wt % NiO/Al_2O_3, and 24 wt % NiO/Al_2O_3.

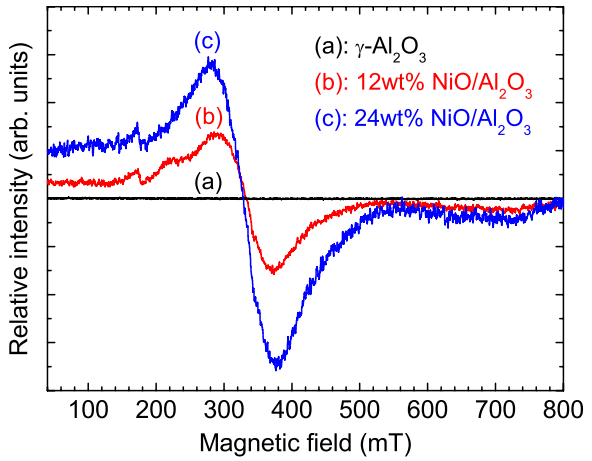

FIG. 10. (Color online) ESR spectra of (a) γ-Al_2O_3, (b) 12 wt % NiO/Al_2O_3, and (c) 24 wt % NiO/Al_2O_3.

Ni $2p_{3/2}$ is about 851.7–853 eV for metallic Ni^0,[24,25] 853.3–855.5 eV for NiO,[24,26,27] 856.1–856.4 eV for Ni_2O_3,[26] and 856.7–857 eV for $NiAl_2O_4$.[25,27] For the samples in the present study, they have been annealed at a low temperature of only 100 °C, therefore Ni_2O_3 or $NiAl_2O_4$ could not be formed in NiO/Al_2O_3 catalysts. Thus we could confirm that Ni species exist in the form of NiO with valence state of 2 +. This is in agreement with the result of XRD measurements. The peak intensities show a strong increase with NiO loading but no clear shift of the peak position was observed. This indicates that no structural change occurred with Ni loading in NiO/Al_2O_3 catalysts.

Mogensen have summarized the Ps reaction with various ions in aqueous solutions.[28] For Ni^{2+} ions, the primary reaction of Ps is spin conversion. Lazzarini *et al.*[29] have systematically studied the spin conversion of Ps by 3*d* metal ions such as V^{2+}, Cr^{2+}, Mn^{2+}, Co^{2+}, and Ni^{2+} ions in solution. These ions could provide unpaired electrons to take part in the spin conversion reaction. The unpaired electrons can be verified by ESR measurements. Saito *et al.* and other researchers also reported the spin conversion of Ps induced by surface paramagnetic centers in UV- and positron-irradiated fine oxide grains at low temperatures.[30–32] They studied the irradiation induced surface paramagnetic centers by ESR, and observed the increasing number of unpaired electrons with increasing irradiation time, which induces the spin conversion of Ps atoms.

The ESR spectra of γ-Al_2O_3, 12 wt % NiO/Al_2O_3 and 24 wt % NiO/Al_2O_3 measured at room temperature are shown in Fig. 10. No ESR signal is observed in γ-Al_2O_3 at room temperature, which is in accordance with the results of Saito *et al.*[30] The ESR signal appears in 12 wt % NiO/Al_2O_3 and 24 wt % NiO/Al_2O_3. This is obviously from the paramagnetic NiO molecules. They have a resonance at ~330 mT. The *g* value can be derived from the formula

TABLE II. Unpaired electron density, o-Ps lifetime τ_4, intensity I_4, and p-Ps intensity $I_{p\text{-}Ps}$ of γ-Al_2O_3, 12 wt % NiO/Al_2O_3 and 24 wt % NiO/Al_2O_3.

Sample	Unpaired electron density (spins/g)	τ_4 (ns)	I_4 (%)	$I_{p\text{-}Ps}$ (%)
γ-Al_2O_3	0	93.7	21.4	10.2
12 wt % NiO/Al_2O_3	2.0×10^{19}	56.3	16.5	12.6
24 wt % NiO/Al_2O_3	6.7×10^{19}	31.7	14.1	15.8

$$h\nu = g\beta H, \tag{5}$$

where *h* is Planck's constant, β is the Bohr magneton, ν is the resonant frequency, and *H* is the applied magnetic field. The obtained *g* value of NiO/Al_2O_3 is around 2.03. The intensity of ESR signal for 24 wt % NiO/Al_2O_3 is higher than that for 12 wt % NiO/Al_2O_3, which implies a higher density of the unpaired electrons in 24 wt % NiO/Al_2O_3.

The unpaired electron densities of the three samples derived from ESR measurement are shown in Table II. In γ-Al_2O_3, no unpaired electron was observed by ESR measurement. The unpaired electron densities of 12 wt % NiO/Al_2O_3 and 24 wt % NiO/Al_2O_3 are higher than that of UV- and positron-irradiated paramagnetic centers (of the magnitude of 10^{17} spins/g).[30] It can be seen from Table II that the p-Ps intensity increases and the o-Ps intensity decreases with the increasing density of unpaired electrons. This confirms the spin conversion of Ps with unpaired electrons of paramagnetic NiO.

IV. CONCLUSION

Positron-annihilation lifetime measurements reveal two long lifetime τ_3 and τ_4 in NiO/Al_2O_3 catalysts, which correspond to o-Ps annihilating in microvoids and large pores, respectively. Both the o-Ps lifetime and its intensity in the large pores show a considerable decrease with increasing NiO content. Meanwhile, the p-Ps intensity, obtained from multi-Gaussian fitting of CDB, increases gradually with NiO content. This confirms the ortho-para conversion of Ps atoms in NiO/Al_2O_3 catalysts. ESR measurements reveal a high density of unpaired electrons in NiO/Al_2O_3 catalysts, which induces the spin conversion of Ps. The present work demonstrates that positronium is a very sensitive probe for the chemical environment at the surface of pores.

ACKNOWLEDGMENTS

This work was supported by the Program for New Century Excellent Talents in University, the National Natural Science Foundation of China under Grants No. 10875088 and No. 10974149, and the 973 program under Grant No. 2008CB617607.

*Corresponding author.
†chenzq@whu.edu.cn
‡sjwangh@yahoo.com.cn

[1] J. A. Azurdia, J. Marchal, P. Shea, H. Sun, X. Q. Pan, and R. M. Laine, Chem. Mater. **18**, 731 (2006).
[2] X. Zhang, J. Liu, Y. Jing, and Y. Xie, Appl. Catal., A **240**, 143 (2003).
[3] M. Trueba and S. P. Trasatti, Eur. J. Inorg. Chem. **2005**, 3393 (2005).
[4] M. Eldrup, D. Lightbody, and J. N. Sherwood, Chem. Phys. **63**, 51 (1981).
[5] P. Asoka-Kumar, M. Alatalo, V. J. Ghosh, A. C. Kruseman, B. Nielsen, and K. G. Lynn, Phys. Rev. Lett. **77**, 2097 (1996).
[6] B. D. Cullity, *Elements of X-Ray Diffraction* (Addison-Wesley, Philippines, 1978), p. 284.
[7] P. Kirkegaard, N. J. Pederson, and M. Eldrup, Ris ϕ National Laboratory, Roskilde, Denmark, 1989.
[8] H. Saito and T. Hyodo, Phys. Rev. Lett. **90**, 193401 (2003).
[9] R. Paulin and G. Ambrosino, J. Phys. (France) **29**, 263 (1968).
[10] C. H. Shek, T. S. Gu, G. M. Lin, and J. K. L. Lai, Appl. Phys. A **66**, 413 (1998).
[11] S. J. Tao, J. Chem. Phys. **56**, 5499 (1972).
[12] H. Nakanishi, S. J. Wang, and Y. C. Jean, in *Positron Annihilation Studies of Fluids*, edited by S. C. Sharma (World Scientific, Singapore, 1988), p. 292.
[13] S. J. Lue, D. T. Lee, J. Y. Chen, C. H. Chiu, C. C. Hu, Y. C. Jean, and J. Y. Lai, J. Membr. Sci. **325**, 831 (2008).
[14] K. Ito, H. Nakanishi, and Y. Ujihira, J. Phys. Chem. B **103**, 4555 (1999).
[15] T. Hyodo, T. Nakayama, H. Saito, F. Saito, and K. Wada, Phys. Status Solidi C **6**, 2497 (2009).
[16] S. Dannefaer and D. Kerr, Nucl. Instrum. Methods **131**, 119 (1975).
[17] G. Dlubek, H. M. Fretwell, and M. A. Alam, Macromolecules **33**, 187 (2000).
[18] A. Alba García, L. D. A. Siebbeles, A. Rivera, H. Schut, S. W. H. Eijt, R. Escobar Galindo, and A. van Veen, Mater. Sci. Forum **363-365**, 287 (2001).
[19] Z. Q. Chen, M. Maekawa, S. Yamamoto, A. Kawasuso, X. L. Yuan, T. Sekiguchi, R. Suzuki, and T. Ohdaira, Phys. Rev. B **69**, 035210 (2004).
[20] Z. Q. Chen, A. Kawasuso, Y. Xu, H. Naramoto, X. L. Yuan, T. Sekiguchi, R. Suzuki, and T. Ohdaira, Phys. Rev. B **71**, 115213 (2005).
[21] H. Nakanishi and Y. C. Jean, in *Positron and Positronium Chemistry*, edited by D. M. Schrader and Y. C. Jean (Elsevier Science, Amsterdam, 1988), p. 159.
[22] Y. C. Jean, Y. Rhee, Y. Lou, H. L. Yen, H. Cao, K. Cheong, and Y. Gu, Phys. Rev. B **54**, 1785 (1996).
[23] *Principles and Application of Positron and Positronium Chemistry*, edited by Y. C. Jean, P. E. Mallon, and D. M. Schrader (World Scientific, Singapore, 2003).
[24] Y. G. Chen and J. Ren, Catal. Lett. **29**, 39 (1994).
[25] Y. Lu, J. Xue, C. Yu, Y. Liu, and S. Shen, Appl. Catal., A **174**, 121 (1998).
[26] B. W. Hoffer, A. D. Langeveld, J. P. Janssens, R. L. C. Bonne, C. M. Lok, and J. A. Moulijn, J. Catal. **192**, 432 (2000).
[27] Z. X. Cheng, X. G. Zhao, J. L. Li, and Q. M. Zhu, Appl. Catal., A **205**, 31 (2001).
[28] O. E. Mogensen, *Positron Annihilation in Chemistry* (Springer-Verlag, Berlin, 1995), p. 183.
[29] A. Fantola-Lazzarini and E. Lazzarini, Coord. Chem. Rev. **213**, 159 (2001).
[30] H. Saito and T. Hyodo, Phys. Rev. B **60**, 11070 (1999).
[31] C. Dauwe and Mbungu-Tsumbu, Phys. Rev. B **45**, 9 (1992).
[32] H. Saito, Y. Nagashima, T. Hyodo, and T. B. Chang, Phys. Rev. B **52**, R689 (1995).